Published in final edited form as:
J Magn Reson Imaging. 2008 September ; 28(3): 612–620. doi:10.1002/jmri.21479.

A Dual-Projection Respiratory Self-Gating Technique for Whole-heart Coronary MRA

Peng Lai[1,2], **Andrew C. Larson**[1,2], **Xiaoming Bi**[3], **Renate Jerecic**[3], and **Debiao Li**[1,2]

[1]Department of Biomedical Engineering, Northwestern University, Chicago, Illinois, USA

[2]Department of Radiology, Northwestern University, Chicago, Illinois, USA

[3]Siemens Medical Solutions, Chicago, Illinois, USA

Abstract

Purpose—To investigate the accuracy of a dual-projection respiratory self-gating (DP-RSG) technique in dynamic heart position measurement and its feasibility for free-breathing whole-heart coronary MR angiography (MRA).

Materials and Methods—A DP-RSG method is proposed to enable accurate direct measurement of heart position by acquiring two whole-heart projections. On 14 volunteers, we quantitatively evaluated the efficacy of DP-RSG by comparison with diaphragmatic navigator (NAV) and single-projection-based respiratory self-gating (SP-RSG) methods. For DP-RSG, we also compared center-of-mass and two profile-matching algorithms in deriving heart motion. Coronary imaging was conducted on 8 volunteers based on retrospective gating to preliminarily validate the effectiveness of DP-RSG for whole-heart coronary MRA. Comparison of vessel delineation was performed between images reconstructed using different gating methods.

Results—The quantitative evaluation shows that DP-RSG more accurately tracks heart motion than NAV with all gating window (GW) values and SP-RSG approaches with GW ≥2.5mm and profile-matching algorithms are more reliable for motion derivation than center-of-mass calculations with GW ≥1.0mm. Whole-heart coronary MRA studies demonstrate the feasibility of using DP-RSG to improve overall delineation of the coronary arteries.

Conclusion—DP-RSG is a promising approach to better resolve respiratory motion for whole-heart coronary MRA compared to conventional NAV and SP-RSG.

Keywords

coronary MRA; respiratory gating; motion correction; self-navigation

INTRODUCTION

Coronary MR angiography (MRA) is emerging as an noninvasive technique for diagnosis of coronary artery diseases. Conventionally, coronary MRA is performed using double-oblique thin slabs targeted at specific coronary artery branches and thus requires precise planning of the imaging plane for each coronary artery branch on each subject (1–3). Due to the tortuous geometry of coronary arteries, visualization is highly dependent on operator skills and ultimately restricted by the slab thickness. Lately, whole-heart coronary MRA was introduced to improve the ease-of-use and the length of vessel depiction (4,5). The complete

Please send proof and correspondence to: Debiao Li, Ph.D., Suite 1600, 737 North Michigan Avenue, Chicago, IL 60611, USA, Tel: (312) 926-4245, Email: d-li2@northwestern.edu.

coronary artery tree is covered in a single measurement and individual branches can be visualized by reformatting the three-dimensional data set retrospectively. However, whole-heart scans require multifold increases in imaging time compared to volume-targeted scans. Despite recent significant advances in MRA, e.g. fast pulse sequences and parallel imaging, the imaging time for high-quality whole-heart coronary MRA is still far beyond breath-hold capabilities and thus necessitates data acquisition during free-breathing.

Free-breathing coronary MRA have been mostly relying upon diaphragmatic navigator (NAV) approaches (4–8). By tracking the motion of the right hemidiaphragmatic dome, respiratory motion of the heart along the superior-inferior (SI) direction can be estimated using a empirical correction factor (typically 0.6) and used for gating and slice tracking (9). NAV approaches are reliant on a simplified motion model assuming: 1) heart motion is linearly related to diaphragmatic motion; 2) a constant correction factor applies to all human subjects. However, as an indirect measurement of heart position, NAV was found susceptible to hysteresis between these two motions (10). Furthermore, a wide variation in the actual correction factor among individuals has been reported (11,12), indicating that usage of a fixed correction factor will result in subject-dependent residual errors in heart position estimates. Additionally, for steady-state free precession (SSFP) sequences widely used for coronary MRA, acquisition of NAV echo is performed prior to steady-state preparation pulses, resulting in significant delays between the acquisition of NAV and imaging data. This long temporal delay can cause out-of-phase measurement of heart position (13). While NAV can suppress motion artifacts sufficiently on many subjects, the above limitations can reduce its effectiveness for coronary MRA within a population with irregular respiratory patterns (11,14).

Recently, an alternative respiratory self-gating (RSG) technique based on direct tracking of heart motion was developed for free-breathing coronary MRA (15,16). For these initial RSG approaches, a one-dimensional (1D) projection of the imaging volume was repeatedly sampled. Respiration-induced heart motion is derived based on either center-of-mass (CM) calculation (15) or profile-shift detection along the 1D projection (16). This single-projection based RSG (SP-RSG) method was reported as a potential approach for more reliable respiratory gating and motion correction than NAV. Nonetheless, the heart is enclosed by the thoracic trunk, which exhibits high signal intensity due to its vicinity to receiver coils and undergoes inconsistent respiratory motion patterns with regard to the heart. Therefore, unavoidably thoracic trunk signals are superimposed with heart signals in the SP-RSG projection and adversely impact the precision of motion derivation.

This paper presents a new dual-projection-based RSG (DP-RSG) method capable of directly tracking SI heart motion immediately before imaging data acquisition without suffering from thoracic trunk signals. Its precision in heart position measurement was evaluated quantitatively in comparison with NAV and SP-RSG. Coronary imaging was also conducted using retrospective gating to preliminarily investigate its feasibility in free-breathing whole-heart coronary MRA on healthy subjects.

THEORY

Respiratory motion of the heart is dominated by a global translation along the SI direction (9). Ideally, breathing-induced heart motion should be directly extracted from profile shifts of the SI projection containing heart signals only. Completely separating heart signals from surrounding thoracic trunk signals is possible by acquiring a 2D heart image in each cardiac cycle. However, the long acquisition time required for collecting gating data would significantly reduce the temporal correlation between the measured heart position and the actual heart position during imaging data acquisition. The DP-RSG method aims to suppress

the undesirable mask of chest wall signals by simply acquiring two SI projections of the whole heart. As shown in Fig.1.a, the first projection is reconstructed from a center *k*-space line in the SI direction and the second is reconstructed from a SI *k*-space line with an additional anterior-posterior (AP) dephasing gradient before readout. The DP-RSG projection, calculated by averaging the two SI projections (Eq. 1), is used for deriving heart motion.

$$\begin{cases} P(x)=\dfrac{c(x,y)\cdot\left[\int\rho(x,y)\cdot dy+\int\rho(x,y)\cdot e^{j\lambda\cdot y}\cdot dy\right]}{2}=\int c(x,y)\cdot\cos(\lambda\cdot y/2)\cdot\left[\rho(x,y)\cdot e^{i\lambda\cdot y/2}\right]dy \\ \lambda=\gamma\cdot G_{ap}\cdot\Delta t_{ap} \end{cases} \quad (1)$$

where *x* and *y* represent SI and AP directions, respectively, $\rho(x,y)$ *and* $c(x,y)$represent the magnetization distribution and coil sensitivity weighting in the imaging slice, respectively, γ is the gyromagnetic ratio, G_{ap} and Δt_{ap} are the amplitude and duration of the AP dephasing gradient, respectively. Clearly, $P(x)$ corresponds to an SI projection of the imaging volume weighted by coil sensitivity and sinusoidal magnitude modulation, $\cos(\lambda\cdot y/2)$, applied along the AP direction. Therefore, for AP signal integration in $P(x)$, artificial bright and dark bands are generated at positions where $\lambda\cdot y/2=2n\pi$ and $(2n+1)\pi$ $(n=0,1,2,3\ldots)$, respectively. The positions of these bands can be determined by changing G_{ap}.

Taking advantage of this AP-position-dependent weighting, the following designs can effectively eliminate chest wall signals while preserving heart signals in $P(x)$: 1) the first bright band ($\lambda\cdot y/2=0$) is centered at heart by setting the AP dephasing coordinate at the heart center; 2) $G_{ap}$is designed such that the first dark band ($\lambda\cdot y/2=\pi$) is positioned at anterior chest wall. Also, only anterior receiver coils are used for both SI projections to attenuate dorsal signals. This method is graphically demonstrated in Fig. 1.b.

MATERIALS AND METHODS

In vivo studies were performed on healthy volunteers to quantitatively evaluate the precision of three respiratory gating techniques, namely, NAV, SP-RSG and DP-RSG, for tracking respiration-induced heart motion. For each measurement, motion signals were derived from the simultaneously recorded NAV echo, SP- and DP-RSG projections and compared to the standard motion characterized by real-time imaging. Furthermore, three algorithms for projection motion derivation were compared to determine a method of choice for DP-RSG. In addition, preliminary comparison with NAV and SP-RSG with regard to vessel delineation was also performed to investigate the effectiveness of DP-RSG for whole-heart coronary MRA.

I. Quantitative Evaluation

Data Acquisition—A 2D single-shot SSFP sequence with electrocardiogram (ECG) triggering was modified for the purpose of quantitative evaluation. To track the SI motion of the heart, a sagittal slice of the heart was imaged during mid-diastole in each cardiac cycle, as show in Fig. 2. GRAPPA was employed to facilitate real-time (RT) data acquisition. To minimize delay time between acquisition of center *k*-space and gating data and meanwhile reduce eddy current effects, a centric-pair trajectory was used in the phase-encoding direction (17). 10 sinusoidal preparation pulses were applied prior to imaging data acquisition to reduce transient signal oscillation (18). For comparison, both NAV echo and DP-RSG *k*-space lines were collected in each cardiac cycle immediately before and after the preparation pulses, respectively. As described in the theory section, for DP-RSG the second projection was acquired with π dephasing in the AP direction.

A total of 14 healthy volunteers (10 males; 4 females) were examined supinely on a 1.5T clinical MRI scanner (MAGNETOM Avanto, Siemens Medical Solutions, Erlangen, Germany). Written informed consent was obtained from each participant before the scan in accordance with our institutional review board. First, low-resolution survey images were acquired in three orthogonal views to determine the positions of the heart and the diaphragm. The distance between the centers of the anterior chest wall and the heart was measured in the survey images and was input to sequence protocol for calculating gradient moments necessary for π AP dephasing. Next, volunteers were scanned using this sequence with simultaneous RT imaging and gating data acquisition. The NAV beam was positioned through the dome of the right hemidiaphragm. A center-heart sagittal slice, localized in the survey scan, was selected for 2D RT imaging. A relatively large slice thickness was used to alleviate the impact of through-plane heart motion in the left-right (LR) direction. The same data acquisition was repeated for 60 heartbeats during free-breathing with the following sequence parameters: 320×200 mm^2 FOV; 12 mm slice thickness; 256×96 matrix; 1.25×2.08 in-plane spatial resolution; TE/TR = 1.6/3.2 ms; 75° flip angle; GRAPPA: acceleration factor of 3 with 24 auto-calibration lines. The total acquisition time for a RT image was ~154ms.

Respiratory Gating Techniques—In each cardiac cycle, a 2D RT image was collected, capturing SI and AP respiratory motion of the heart during the scan. NAV and DP-RSG projections were reconstructed from the NAV echo and the average of the two RSG *k*-space lines, respectively. Also, from the first RSG *k*-space line, a 1D projection of the imaging volume could be calculated and used for SP-RSG.

2D respiratory motion was extracted by tracking global SI and AP translations of the heart profile in the RT images. Similarly, respiratory gating signals, representing the SI motion of the heart during a scan, were derived from the repeatedly measured NAV echo and RSG data by detecting the shift of target profile in the corresponding projections. Correlation coefficient (CC) as will be described was used for all profile matching and the following two steps were followed for motion detection. First, the RT images in the beginning 15 cardiac cycles were visually assessed and an end-expiration heartbeat was selected as the reference heartbeat. In order to maintain the same position baseline for all the motion signals, the RT image, NAV and RSG projections acquired in the same reference heartbeat were selected to generate templates for profile matching: the region of the heart in the reference RT image was manually defined and the template image was generated by eliminating the signal outside this region; correspondingly, only the signal within the SI window covering the heart in the reference SP- and DP-RSG projections was selected as the SP- and DP-RSG templates, respectively; similarly, a narrow window covering the diaphragm-lung interface in the NAV projections was visually identified and the signal within the window in the reference NAV projection was selected as the NAV template. Next, diaphragm motion and heart motion were estimated by matching each RT image, NAV and RSG projections with the corresponding templates. For NAV, detected diaphragmatic displacements were multiplied by a correction factor of 0.6 to estimate heart motion (9).

Motion Derivation Algorithms—For DP-RSG, respiratory motion was estimated by detecting the signal change in the projection. Three commonly used motion derivation algorithms were investigated in this work, namely, CM, CC and least squares (LS).

CM: As a first-moment measurement of target position, CM of the RSG projection is a direct reflection of the SI position of the heart (15). In this work, in order to reduce the effects of surrounding tissues undergoing different motion patterns, e.g. diaphragm and liver, only signals within the window covering the heart were included for CM calculation, as illustrated in Eq. 2.

$$D=\frac{\sum_{x\in W}P(x)\cdot x}{\sum_{x\in W}P(x)}-\frac{\sum_{x\in W}T(x)\cdot x}{\sum_{x\in W}T(x)} \quad (2)$$

where D is the estimated heart displacement, x represents the SI direction, Windicates the heart window in the RSG projection and $T(x)$ represents the reference RSG projection.

CC: SI motion of the heart also manifests as profile shifts in the RSG projection. Therefore, algorithms detecting such shifts by matching a projection with the reference could be used for heart position measurement (16). A commonly used algorithm based on maximizing CC is illustrated in Eq.3. CC was calculated as the degree of matching with a range of displacements, Δx, and the Δx producing the maximum CC was regarded as the estimated heart displacement.

$$\begin{cases} D=\arg\max_{\Delta x} Corr(\Delta x) \\ Corr(\Delta x)=\dfrac{\sum_{x\in W}[P(x-\Delta x)-\overline{P}]\cdot[T(x)-\overline{T}]}{\left\{\sum_{x\in W}[P(x-\Delta x)-\overline{P}]^2\cdot\sum_{x\in W}[T(x)-\overline{T}]^2\right\}^{1/2}} \end{cases} \quad (3)$$

where, $\overline{P}$ and $\overline{T}$ are the mean values of $P(x)$ and $T(x)$ within W, respectively.

Heart motion in RT images was also detected using CC by extending the preceding method to two dimensions. The CC value of a RT image with the reference image was calculated in a range of 2D displacements in SI and AP directions. The estimated 2D heart motion corresponds to the 2D displacement generating the maximum CC value.

LS: Alternatively, profile matching could also be performed by minimizing the deviation between a projection and the reference. According to Eq. 4, a set of Δx values were tested and the one corresponding to the minimum deviation was taken as the displacement estimate. Due to the unavoidable heart rate variations, the time interval for signal recovery is not identical in different cardiac cycles and therefore the amplitude of the RSG projection fluctuates during a scan. Unlike CC with intrinsic signal normalization, conventional LS is sensitive to such signal fluctuation. In this regard, an adapted LS definition was used, where $P(x)$ and $T(x)$ were both normalized based on the energy within W.

$$\begin{cases} D=\arg\min_{\Delta x} Dev(\Delta x) \\ Dev(\Delta x)=\sum_{x\in W}\left[\dfrac{P(x-\Delta x)}{\sqrt{\sum_{x\in W}P(x-\Delta x)^2}}-\dfrac{T(x)}{\sqrt{\sum_{x\in W}T(x)^2}}\right]^2 \end{cases} \quad (4)$$

Analysis—For each volunteer, the SI component of the 2D RT motion signal was used as the standard for accuracy assessment. The absolute error of a gating method or a motion derivation algorithm was estimated by calculating the absolute deviation of the corresponding motion signal from the standard motion signal. The absolute errors of

different motion signals were compared within different gating windows, defined as the range of the actual heart displacement estimated from RT imaging. Specifically, for a gating window of A mm, all the absolute errors in those cardiac cycles with a displacement within ±A were selected for analysis. For a fair comparison based on the same scan efficiencies, the precision of different respiratory gating techniques and motion derivation algorithms was evaluated by comparing the absolute errors with the same gating windows. One-way ANOVA was used to test the overall difference among these measurements and next paired t-test was used for pair-wise comparisons between each two gating techniques or motion derivation algorithms. For all the tests above, a p value smaller than 0.05 was regarded as significant.

II. Whole-heart Coronary MRA

Preliminary whole-heart coronary MRA was performed based on retrospective respiratory gating. The sequence used for coronary imaging was similar to that for quantitative evaluation, except for the following changes. First, 3D segmented data acquisition, rather than 2D single-shot acquisition, was performed in a sagittal volume covering the entire heart and each segmented data acquisition was repeatedly sampled for 4 times to approximately cover a respiratory cycle. Furthermore, T2-preparation and spectrally selective pulses were applied before each segmented data acquisition to enhance blood-myocardium contrast and suppress fat signals, respectively (4). Additionally, 3D *k*-space lines were collected using a centric-pair order in the phase-encoding direction similar to the quantitative evaluation sequence and a linear order in the partition-encoding direction.

Coronary MRA was conducted on 8 healthy volunteers (5 males; 3 females) after obtaining written informed consent from each of them. Data acquisition was performed during mid-diastole. Each scan started with a 5 second end-expiration breath hold. The NAV echo and RSG *k*-space lines collected in the third heartbeat were used to generate profile-matching templates which were used throughout the scan for motion derivation. The imaging parameters included: 320×250 mm^2 FOV; 60 slices interpolated into 120 slices with 1.1 mm thickness; 320×210 matrix; 1.0×1.2 in-plane spatial resolution; 38 lines/segment; 75° flip angle; TE/TR = 1.87/3.74 ms, GRAPPA: acceleration factor of 2 with 28 auto-calibration lines.

Respiratory motion signals, namely, NAV, SP- and DP-RSG motion signals, were derived from the simultaneously acquired NAV echo and RSG data. Next, three image sets were reconstructed from each raw dataset using NAV gating, SP- and DP-RSG, respectively. All reconstructions were performed based on conventional retrospective respiratory gating: among the four successive measurements of a *k*-space segment, the one with a heart position most consistent with the reference position was accepted; SI translational motion was corrected for each *k*-space segment by applying a linear phase modulation based on the estimated heart displacement in the corresponding cardiac cycle (19).

For evaluation of vessel delineation, NAV, SP- and DP-RSG image sets from each volunteer were reformatted in identical orientations providing best visualizations of the left anterior descending (LAD) and the right coronary artery (RCA). For each volunteer, the LAD and RCA images reconstructed were displayed in two separate slides. In each slide, the images reconstructed using NAV, SP- and DP-RSG were shown in a row with the order of placement randomized. All the images were scored independently by two cardiac MR specialists blinded to the reconstruction method on a 5 point scale with regard to coronary artery depiction (4: excellent; 3: good; 2: acceptable; 1: poor; 0: undistinguishable). For each image, the average score from the two reviewers was regarded as the qualitative evaluation of vessel delineation. A comparison between the three techniques in overall coronary artery

delineation was performed based on both RCA and LAD scores using a Wilcoxon signed rank test (significance level = 0.05).

RESULTS

Quantitative Evaluation

For each of the 14 volunteer studies, respiratory motion of the heart was assessed in the RT images, NAV and RSG projections. A representative example is shown in Fig. 3. The right hemidaphragmatic dome, indicated by the region within the dashed lines in the time-series plot of the NAV projection (Fig. 3.a), clearly exhibits a respiratory motion pattern. Visually, the simultaneously recorded heart motion, demonstrated as profile shifts within the dashed lines in the RSG projections (Fig. 3.b and c), is synchronized with diaphragmatic motion. Furthermore, the heart profile is better depicted in the DP-RSG projection with sharper upper and lower edges compared to the SP-RSG projection with superimposed chest wall signals obscuring the heart profile. Fig 4.a shows a section of the SI heart motion derived using different respiratory gating techniques from the same volunteer. Clearly, the four motion signals are highly synchronous in the temporal dimension, while exhibiting significant discrepancy in magnitude. With reference to the standard motion characterized by RT imaging, the DP-RSG motion signal follows the SI respiratory motion of the heart closely throughout the scan, as opposed to the overestimation of heart motion apparent for both NAV and SP-RSG. Fig 4.b shows the SI heart motion extracted from the DP-RSG projection using different derivation algorithms. We can see that CC and LS generate very similar motion signals. In contrast, heart motion is considerably underestimated using CM.

Fig. 5 shows the mean absolute errors for different gating techniques and motion derivation algorithms with a range of gating windows. One-way ANOVA reveals that there is a significant difference between different gating techniques and motion derivation algorithms for all GW's. According to the pair-wise tests, the absolute errors of DP-RSG are always significantly lower than NAV ($p<0.05$). The absolute errors of SP-RSG and DP-RSG are comparable with gating windows ≤ 2mm. However, with larger GW, SP-RSG becomes significantly less accurate than DP-RSG ($p<0.05$). Comparing the three derivation algorithms, the difference between CC and LS is not significant, and CM produces significantly larger errors than CC and LS with GW ≥1.0mm ($p<0.05$).

Whole-heart Coronary MRA

Fig. 6 shows the LAD and RCA images reconstructed using different gating schemes. Compared to the nongated images, in which both coronary arteries are almost undistinguishable, NAV and DP-RSG significantly reduce motion artifacts and produce similar coronary artery depiction. In comparison, the residual motion artifacts in the SP-RSG images remain significant and obscure visualization of the coronary arteries. Fig. 7 shows a case in which DP-RSG achieves higher image quality than the other two schemes. As indicated by the arrows, the medial segment of RCA is better delineated in the DP-RSG image (Fig. 7.a) than in the NAV (Fig. 7.b) and SP-RSG (Fig. 7.c) images. The improvement is more clearly illustrated in the corresponding zoomed image slices covering this coronary segment (Fig. 7.d~f). The averaged image scores from all 8 subjects are shown in table 1. By comparing DP-RSG and NAV scores, the former is equal to the latter in 4 cases, are lower in 3 cases and are higher in 9 cases. By comparing the two RSG methods, DP-RSG ties with SP-RSG in 2 cases, is inferior in 1 case and superior in 13 cases. Overall, the mean scores of NAV, SP-RSG and DP-RSG are 2.69±0.64, 2.57±0.63 and 2.83±0.58, respectively. Statistically, DP-RSG receives significantly higher scores than both NAV and SP-RSG ($p<0.05$), while the difference between NAV and SP-RSG is insignificant.

DISCUSSION

For coronary MRA using SSFP sequences, blood signals are of relatively high intensity due to the intrinsic bright blood feature of SSFP. T2-preparation and fat-saturation pulses applied prior to each segmented data acquisition further enhance the contrast of coronary blood to surrounding tissues. Therefore, the heart usually exhibits a hyper-intense profile in the 1D projection of the imaging volume and its motion is reflected by profile shifts within this projection. This feature enables SP-RSG based on acquisition of a center *k*-space line. However, surrounding chest wall signals inevitably superimpose onto the 1D projection and can adversely affect the precision of SP-RSG. The proposed DP-RSG method can resolve this problem by simply collecting one additional k-space line. With effective chest wall suppression, an SI projection containing primarily heart signal can be repeatedly sampled and used for motion tracking. Superiority of DP-RSG in resolving respiratory motion for whole-heart coronary MRA compared to SP-RSG was validated by our quantitative and qualitative evaluations.

In this work, quantitative accuracy and qualitative image score comparisons were performed between DP-RSG and conventional NAV. It has been shown that DP-RSG measures SI respiratory motion of the heart more accurately than NAV and provides the feasibility for an overall improvement in vessel delineation for whole-heart coronary MRA. Potential improvements can be most likely attributed to two advantageous features of this RSG method. First, respiratory motion is directly measured from the heart and thus is self-adapted to the motion pattern of the specific subject under study. Furthermore, acquisition of the two SI projections for DP-RSG does not disturb steady state signal and can be performed immediately preceding center *k*-space sampling. Therefore, the temporal delay between gating and imaging is minimized, as opposed to the long delay (> 60 ms) for NAV.

Quantitative comparison was also performed between three motion derivation algorithms. Noticeably, the precision of CM is significantly lower than the profile-matching methods. Although chest wall signals are suppressed, the heart is not a completely separate object in the DP-RSG projection but connected with nonzero peripheral signals superior and inferior to the heart, e.g. abdominal signals. Therefore, the calculated CM shift is not only determined by heart motion but also impacted by the peripheral signals moving into and out of the heart window *W*. In most cases, CM tends to underestimate the true SI heart motion. In contrast, CC and LS produced mean errors ≤0.35 mm within a heart motion range of ±3 mm and thus are methods of choice for motion derivation.

Although proposed only for single-frame coronary MRA, DP-RSG is potentially also suitable for many time-resolved whole-heart imaging applications, such as whole-heart cine imaging, phase-contrast flow measurement and 4D coronary MRA. Acquisition of NAV echo necessitates a halt of about 20 ms and therefore has very limited compatibility with cine SSFP imaging. Contrarily, DP-RSG requires a relatively minor overhead of 2 TR's (≈7ms) while maintaining the steady state of SSFP signal. Furthermore, the gradients for the two SI projections are almost identical except for slight differences in the AP gradient. With this intrinsic pairing, the DP-RSG approach should be able to reduce the eddy-current-related signal oscillation in cine SSFP imaging compared to interleaved acquisition of a single center *k*-space line (17). Further studies are needed to investigate its effects in this regard.

Applying regional saturation pulses is an alternative method for chest wall suppression (15). However, SP-RSG with regional saturation has a few disadvantages compared to DP-RSG. First, for SSFP sequences, inserting acquisition of a single RSG k-space line prior to imaging data acquisition can disturb steady state magnetization established during dummy

radiofrequency (RF) cycles and induce eddy current artifacts as observed in our initial studies. Second, T1-dependent magnetization recovery in the saturated region would occur during dummy RF cycles, resulting in incomplete chest wall suppression for self-gating. Third, imprecise placement of the saturation band as well as the imperfect slice-selection profile of the saturation pulse may interfere with visualization of the medial segment of RCA, which is usually in vicinity to the anterior chest wall. Additionally, usage of regional saturation pulses prohibits extension of this method to cine SSFP data acquisition. In comparison, the dual-projection method can suppress chest wall signals without affecting coronary imaging and is SSFP compatible. In this work, direct comparison was not performed between these two methods, because, otherwise, it would be infeasible to distinguish chest wall suppression effects due to the regional saturation pulse and the second RSG projection.

2D selective-excitation pulses also enable direct monitor of heart motion by placing a pencil-beam echo on a heart region free of coronary arteries. However, an early comparison study has shown that this method is inferior to diaphragmatic navigator (20). Possible reasons include: 1. to avoid interference with coronary imaging, the pencil-beam diameter needs to be very small, resulting in reduced SNR of the navigator echo; 2. local motion detected at a small spot on the heart wall may be inconsistent with the global motion of the entire heart; 3. this method is very sensitive to the shift of the actual tracking spot during a scan induced by heart translation in transverse directions and heart deformation due to heartbeat variations. In contrast, the proposed RSG method measures the profile shift of the entire heart, which should be more consistent with the global motion of the entire coronary artery tree.

As can be noticed in Eq 1, there is an AP phase modulation item, $e^{j\lambda \cdot y/2}$, in the DP-RSG projection formula. This phase variation may introduce signal cancellation in $P(x)$ when integrating signals along the AP direction. However, because the small AP dephasing needed for chest wall suppression does not cause large phase variations in the heart region ($<\pi$), the heart profile remains well preserved in the DP-RSG projection. Also, this phase variation can be eliminated by sampling the two SI projections with $\pi/2$ and $-\pi/2$ AP dephasing rather than with 0 and π AP dephasing. These two schemes were compared in our initial studies, generating similar results in heart position measurement. The latter was selected in this study simply to facilitate a direct comparison between motion derivation based on the average projection for DP-RSG and the first projection alone for SP-RSG. By this means, the effects of adding the second SI projection could be investigated.

Many earlier studies have demonstrated that breathing also causes nonrigid heart deformation. Typically, superior cardiac regions move less than inferior regions during tidal breathing (21). Therefore, motion compensation based on global translation introduces residual region-dependent displacements for whole-heart coronary MRA. This nonrigid feature was also observed in our human studies. As shown in Fig 3.c, the shift of the upper edge of the heart profile is distinguishably smaller than that of the lower edge. This implies the possibility of characterizing nonrigid heart motion by detecting the SI stretching in the DP-RSG projection such that residual motion artifacts can be reduced. For this purpose, the motion derivation algorithm should be improved to fit for a more general motion model encompassing SI translation and stretching.

In this work, sagittal orientation was used for whole-heart coronary MRA with frequency encoding in the SI direction, while conventional whole-heart protocols use transverse orientation with a left-right frequency-encoding direction (4,5). The former orientation was chosen such that steady state signal could be easily maintained during consecutive acquisition of the DP-RSG projection along the SI direction and imaging data. As observed

in our 8 volunteer studies, thickness of a sagittal whole-heart slice could be either slightly larger or slightly smaller than that for a transverse slice, depending on the heart geometry of the subject. However, it should be noted that this RSG technique does not necessarily require sagittal imaging orientation. Since the entire heart is covered by the imaging volume for whole-heart coronary MRA, an SI projection of the heart can also be measured for real-time tracking of SI heart motion with conventional transverse orientation. By this means, imaging orientation can be more flexibly determined so as to minimize slice thickness and thus reduce imaging time.

Retrospective gating was currently used to resolve respiratory motion for whole-heart coronary MRA. The reason of using this scheme in our study was that NAV, SP-RSG and DP-RSG images could be reconstructed from the same raw *k*-space datasets such that a fair comparison could be performed between these competing techniques, exempted from effects of interscan changes in heart rates and respiratory motion. Nonetheless, retrospective gating usually retains considerable residual motion artifacts (22). In consequence, the coronary images obtained in this study are of relatively lower quality compared to prospective gating images, which discouraged further evaluations. For this reason, only grading of vessel delineation was performed for comparison. Future work should conduct a more complete comparison between these techniques based on prospective gating. In that scenario, the tradeoff between image quality and scan efficiency must be considered. Since the correlation between true SI heart motion and detected motion varies significantly among different gating methods, on each subject the gating window should be determined individually for NAV, SP- and DP-RSG scans to maintain similar acceptance ratios for these scans.

CONCLUSION

The presented work demonstrated the principle of a new DP-RSG method and validated its superior heart position measurement compared to conventional NAV and SP-RSG. Preliminary comparison with NAV and SP-RSG based on vessel delineation also illustrated that DP-RSG is promising for free-breathing whole-heart coronary MRA. Among the three derivation algorithms evaluated, either CC or LS is more reliable than CM and should be used for future DP-RSG implementation. Further studies are in progress to extend this technique for more comprehensive motion detection and to fully investigate its effectiveness in whole-heart coronary MRA.

Acknowledgments

Supported in part by National Institute of Health grants no. NIBIB EB002623 and no. NHLBI HL079148 and Siemens Medical Solutions USA, Inc., Malvern, PA

REFERENCES

1. Manning WJ, Li W, Boyle NG, Edelman RR. Fat-suppressed breath-hold magnetic resonance coronary angiography. Circulation. 1993; 87(1):94–104. [PubMed: 8419029]
2. Botnar RM, Stuber M, Danias PG, Kissinger KV, Manning WJ. Improved coronary artery definition with T2-weighted, free-breathing, three-dimensional coronary MRA. Circulation. 1999; 99(24): 3139–3148. [PubMed: 10377077]
3. Deshpande VS, Shea SM, Laub G, Simonetti OP, Finn JP, Li D. 3D magnetization-prepared true-FISP: a new technique for imaging coronary arteries. Magn Reson Med. 2001; 46(3):494–502. [PubMed: 11550241]
4. Weber OM, Martin AJ, Higgins CB. Whole-heart steady-state free precession coronary artery magnetic resonance angiography. Magn Reson Med. 2003; 50(6):1223–1228. [PubMed: 14648570]

5. Bi X, Deshpande V, Carr J, Li D. Coronary artery magnetic resonance angiography (MRA): a comparison between the whole-heart and volume-targeted methods using a T2-prepared SSFP sequence. J Cardiovasc Magn Reson. 2006; 8(5):703–707. [PubMed: 16891229]
6. Li D, Kaushikkar S, Haacke EM, Woodard PK, Dhawale PJ, Kroeker RM, Laub G, Kuginuki Y, Gutierrez FR. Coronary arteries: three-dimensional MR imaging with retrospective respiratory gating. Radiology. 1996; 201(3):857–863. [PubMed: 8939242]
7. Wang Y, Rossman PJ, Grimm RC, Riederer SJ, Ehman RL. Navigator-echo-based real-time respiratory gating and triggering for reduction of respiration effects in three-dimensional coronary MR angiography. Radiology. 1996; 198(1):55–60. [PubMed: 8539406]
8. Danias PG, McConnell MV, Khasgiwala VC, Chuang ML, Edelman RR, Manning WJ. Prospective navigator correction of image position for coronary MR angiography. Radiology. 1997; 203(3): 733–736. [PubMed: 9169696]
9. Wang Y, Riederer SJ, Ehman RL. Respiratory motion of the heart: kinematics and the implications for the spatial resolution in coronary imaging. Magn Reson Med. 1995; 33(5):713–719. [PubMed: 7596276]
10. Nehrke K, Bornert P, Manke D, Bock JC. Free-breathing cardiac MR imaging: study of implications of respiratory motion--initial results. Radiology. 2001; 220(3):810–815. [PubMed: 11526286]
11. Danias PG, Stuber M, Botnar RM, Kissinger KV, Edelman RR, Manning WJ. Relationship between motion of coronary arteries and diaphragm during free breathing: lessons from real-time MR imaging. AJR Am J Roentgenol. 1999; 172(4):1061–1065. [PubMed: 10587147]
12. Taylor AM, Keegan J, Jhooti P, Firmin DN, Pennell DJ. Calculation of a subject-specific adaptive motion-correction factor for improved real-time navigator echo-gated magnetic resonance coronary angiography. J Cardiovasc Magn Reson. 1999; 1(2):131–138. [PubMed: 11550345]
13. Spuentrup E, Manning WJ, Botnar RM, Kissinger KV, Stuber M. Impact of navigator timing on free-breathing submillimeter 3D coronary magnetic resonance angiography. Magn Reson Med. 2002; 47(1):196–201. [PubMed: 11754460]
14. Stehling, MK.; Balci, C.; Reiser, M. Navigator Echo Coronary MRA: Controversial Results. Proceedings of the 5th Annual Meeting of ISMRM; Vancouver, Canada. 1997. p. 911
15. Stehning C, Bornert P, Nehrke K, Eggers H, Stuber M. Free-breathing whole-heart coronary MRA with 3D radial SSFP and self-navigated image reconstruction. Magn Reson Med. 2005; 54(2):476–480. [PubMed: 16032682]
16. Lai, P.; Larson, AC.; Park, J.; Carr, JC.; Li, D. Respiratory Self-Gated 4D Coronary MRA. Proceedings of the 14th Annual Meeting of ISMRM; Seattle, USA. 2006. p. 364
17. Bieri O, Markl M, Scheffler K. Analysis and compensation of eddy currents in balanced SSFP. Magn Reson Med. 2005; 54(1):129–137. [PubMed: 15968648]
18. Paul, D.; Hennig, J. Comparison of different flip angle variation functions for improved signal behavior in SSFP sequences. Proceedings of the 12th Annual Meeting of ISMRM; Kyoto, Japan. 2004. p. 2663
19. Ehman RL, Felmlee JP. Adaptive technique for high-definition MR imaging of moving structures. Radiology. 1989; 173(1):255–263. [PubMed: 2781017]
20. Stuber M, Botnar RM, Danias PG, Kissinger KV, Manning WJ. Submillimeter three-dimensional coronary MR angiography with real-time navigator correction: comparison of navigator locations. Radiology. 1999; 212(2):579–587. [PubMed: 10429721]
21. Nagel E, Bornstedt A, Schnackenburg B, Hug J, Oswald H, Fleck E. Optimization of realtime adaptive navigator correction for 3D magnetic resonance coronary angiography. Magn Reson Med. 1999; 42(2):408–411. [PubMed: 10440967]
22. Du YP, McVeigh ER, Bluemke DA, Silber HA, Foo TK. A comparison of prospective and retrospective respiratory navigator gating in 3D MR coronary angiography. Int J Cardiovasc Imaging. 2001; 17(4):287–294. discussion 295-286. [PubMed: 11599868]

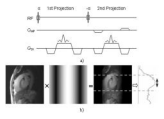

Figure 1.

a) Sequence diagram for DP-RSG data acquisition. b) Graphical presentation of the DP-RSG method. The left figure is a center-slice image reconstructed using only the anterior receiver coil. Note the significant attenuation of dorsal signals. The second figure illustrates the sinusoidal magnitude modulation in the AP direction in Eq. 1. The dark and bright bands are positioned at the anterior chest wall and the heart, respectively, such that the average projection contains primarily signals originating from the heart (region between the two dashed-lines) as shown within projection at the right.

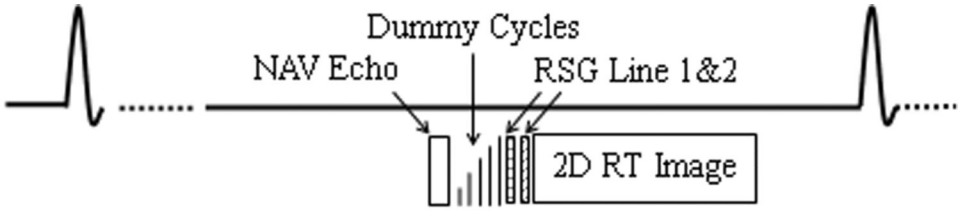

Figure 2.
Schematic diagram of the pulse sequence used to quantify the accuracy of NAV and RSG respiratory motion tracking.

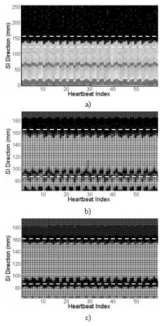

Figure 3.
Time-series plots of a) NAV projection, b) SP-RSG projection, and c) DP-RSG projection acquired in a free-breathing scan. The dashed lines in a) indicate the diaphragm-lung interface. The dashed lines in b) and c) indicate the window covering the heart in the SI direction.

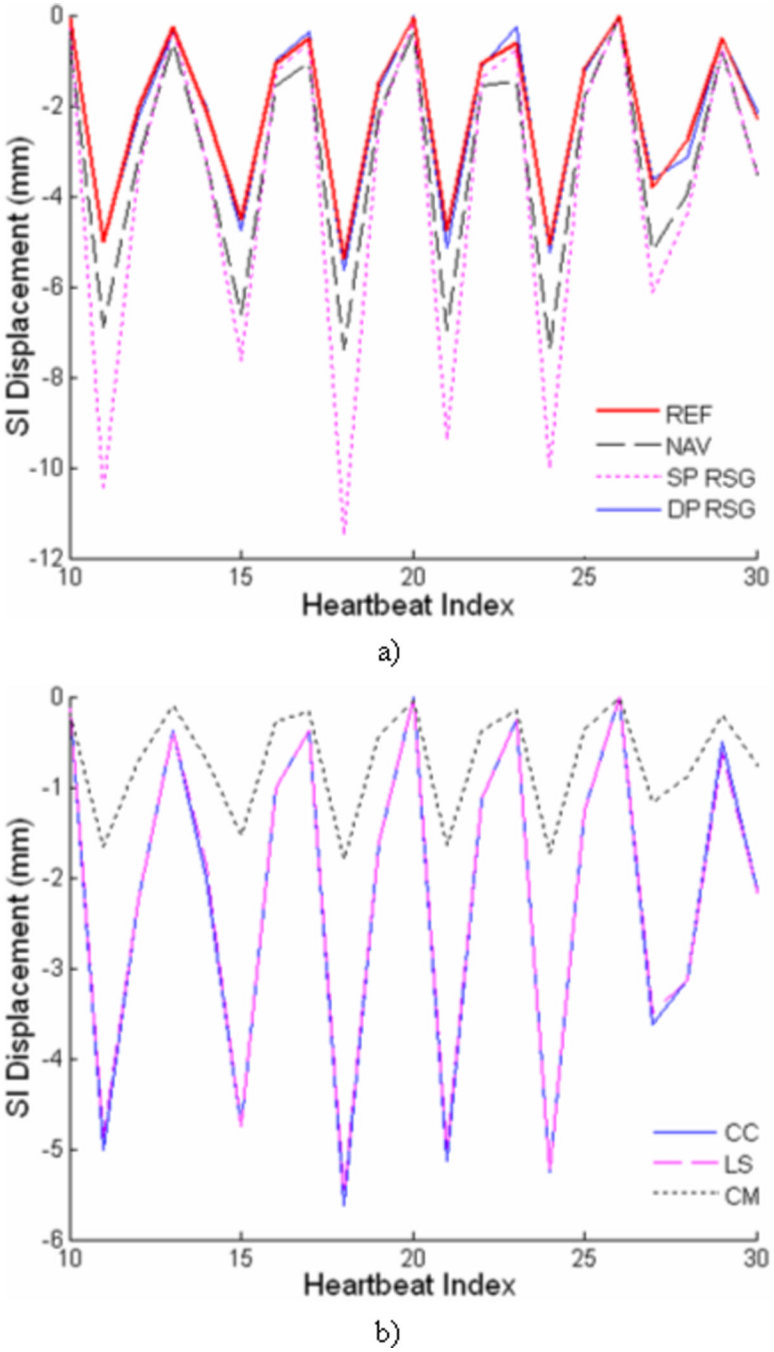

Figure 4.
A representative time series of the heart motion signals derived using a) different respiratory gating techniques and b) motion derivation algorithms.

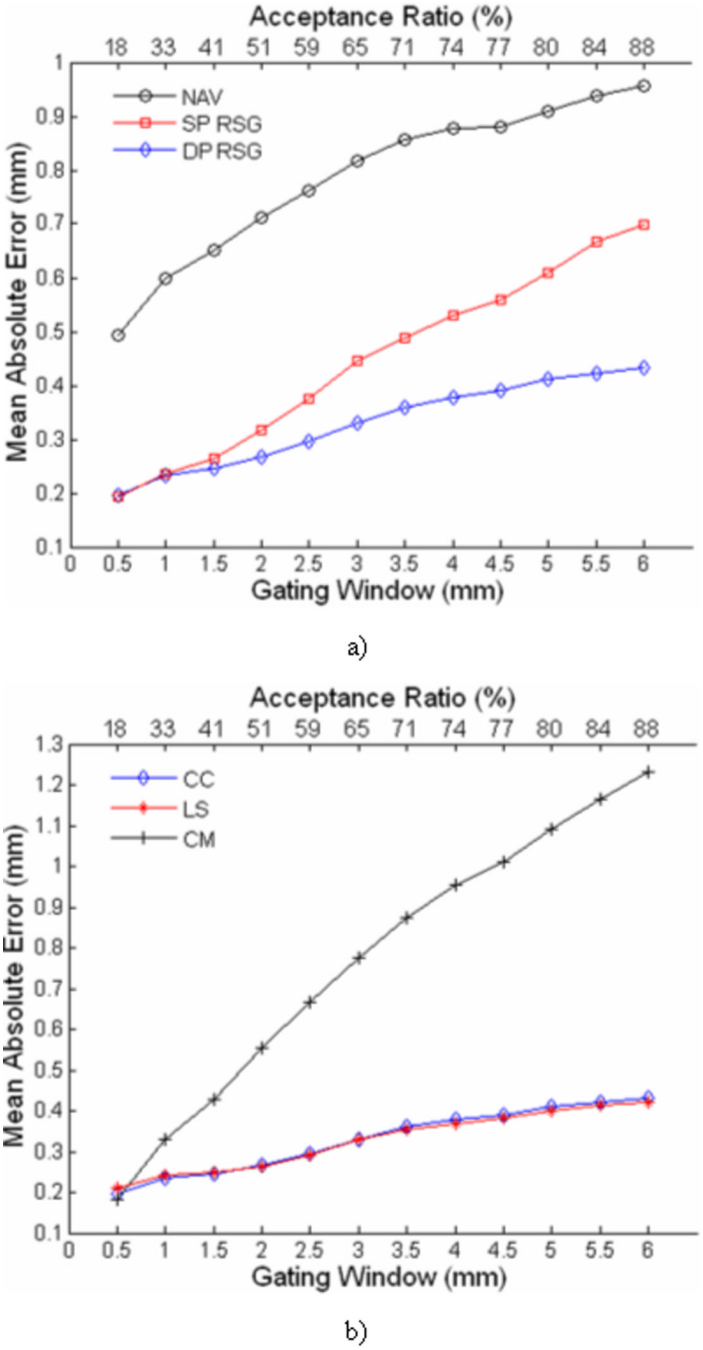

Figure 5.
The mean absolute errors of different respiratory gating techniques (a) and motion derivation algorithms (b) with a range of gating windows. The upper horizontal axis shows the average acceptance ratios achieved with the corresponding gating windows in the lower horizontal axis.

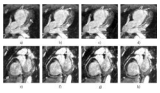

Figure 6.
(a–d) show the LAD images reconstructed without gating and using NAV, SP-RSG and DP-RSG, respectively. (e–h) show the RCA images reconstructed without gating and using NAV, SP-RSG and DP-RSG, respectively. Note the severe vessel blurring in the non-gated images, as indicated by the arrows.

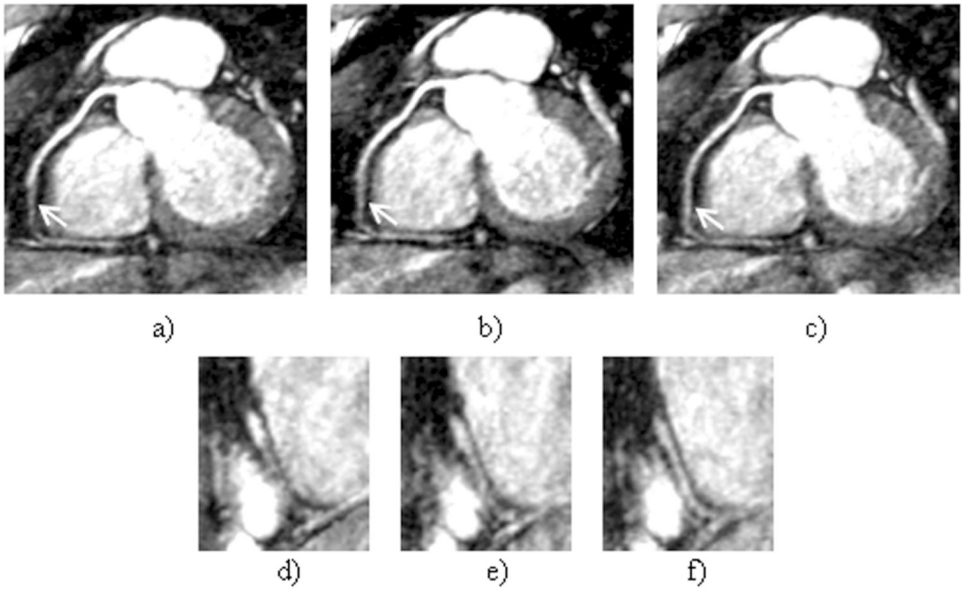

Figure 7.
a~c) are the reformatted images of RCA reconstructed using NAV, SP-RSG and DP-RSG, respectively. d~f) are the zoom-in regions in the corresponding sagittal slices covering the coronary artery segment indicated by the arrows in a~c), respectively.

Table 1

Scores of the LAD and RCA images reconstructed using different gating methods

Subject Index		1	2	3	4	5	6	7	8
LAD	NAV	3.25	1.50	3.10	1.50	2.25	2.55	2.85	3.00
	SP-RSG	2.85	1.20	2.80	1.75	1.90	2.95	2.50	3.00
	DP-RSG	3.25	1.75	3.25	1.90	2.40	2.80	2.65	3.00
RCA	NAV	3.60	2.00	3.00	3.05	2.30	2.50	3.10	3.50
	SP-RSG	2.95	2.40	3.10	2.40	1.95	2.50	3.10	3.70
	DP-RSG	3.60	2.60	3.25	2.95	2.10	2.95	3.10	3.80